Supporting Information

Kiser et al. 10.1073/pnas.0906600106

SI Methods

Purification of RPE Membranes Containing RPE65. Fresh bovine eyes, obtained from a local slaughter house (Mahan Packing), were hemisected and retinas were removed. Approximately 1 mL of 48 mM sodium MOPS, pH 7.0, containing 0.25 M sucrose and 1 mM DTT was added to each eyecup, the RPE cell layer was detached by brushing, and the resultant cell suspension was filtered through cotton gauze to remove large particulate matter and stored at −80 °C until needed. RPE microsomes were prepared as described with some modifications (1). Briefly, the RPE cell suspension was thawed in a 33 °C water bath, and cells were disrupted by dounce homogenization. The lysate was centrifuged at 20,000 × *g* for 20 min to pellet choroidal material, unbroken cells, and large organelles. The supernatant was removed and centrifuged at 100,000 × *g* for 75 min to pellet microsomal membranes. The supernatant was removed, and the microsomes were rinsed with deionized water and then incubated in ≈12 mL of 10 mM Tris acetate, pH 7.0, containing 1 mM DTT and 1 M KCl on ice for 1 h to remove peripherally bound membrane proteins. The microsomes were then harvested by centrifugation at 100,000 × *g* for 1 h and again rinsed with deionized water. All centrifugations in this study were performed at 4 °C.

Purification of RPE65 from KCl-Washed RPE Microsomes. RPE microsomes were resuspended in ≈12 mL of 10 mM Tris acetate, pH 7.0, containing 1 mM DTT and 24 mM n-octyltetraoxyethylene (C_8E_4) (Anatrace) and allowed to incubate on ice for 1 h. The mixture was centrifuged at 100,000 × *g* for 1 h to pellet insoluble material. RPE65 was purified from the supernatant by anion-exchange chromatography on a 1-mL DEAE-Macroprep column (Bio-Rad) preequilibrated with 10 mM Tris acetate, pH 7.0, containing 16 mM C_8E_4 and 1 mM DTT. The column was washed with 5 mL of the same buffer, and the protein was eluted with a 0–500 mM linear NaCl gradient. RPE65 eluted from the column at an approximate conductance of 20 mS/cm. Fractions containing RPE65 were pooled and concentrated to 10–15 mg protein/mL in a 50-kDa molecular weight cutoff Amicon centrifugal filter (Millipore). The concentrated protein solution (typically, 100–200 μL total volume), which exhibited a pronounced reddish brown hue, was then dialyzed overnight against 50 mL of 10 mM Tris acetate, pH 7.0, containing 1 mM DTT and 19.2 mM C_8E_4 to remove excess detergent and salt. The resulting protein preparation was used directly for crystallization trials and biochemical experiments. It was noted that a significant amount of retinoids, primarily retinyl esters, copurified with RPE65. Exogenous iron was not added at any time during purification or crystallization trials. On average we obtained 150 μL of protein solution at a concentration of 10–15 mg/mL and a purity of 90–95%, as judged by Coomassie-stained gels, from 300 adult bovine eyes. Column chromatography was performed at 4 °C.

Gel Filtration Chromatography. Purified RPE65 at an approximate concentration of 5 mg/mL was loaded onto a Superdex 200 10/300 gel filtration column (Amersham Biosciences) equilibrated with 10 mM Tris acetate, pH 7.0, containing 150 mM NaCl, 1 mM DTT and 19.2 mM C_8E_4. The column was developed at a flow rate of 0.5 mL/min in a buffer identical to the equilibration buffer. Bio-Rad gel filtration standards, which were separated under conditions identical to those of RPE65, were used to calibrate the column so that the apparent molecular mass of RPE65 could be quantified.

RPE65 Crystallization. RPE65 crystals were grown by the hanging-drop vapor diffusion method by mixing 1 μL of protein solution with either 1 μL of 0.3 M sodium acetate, pH 8.0, containing 11% wt/vol PEG 3350 (condition A) or 1 μL of 100 mM sodium MES, pH 6.0, containing 30% vol/vol PEG 200 and 2 mM DTT (condition B) at room temperature and incubating the drops over 0.5 mL of the same crystallization solution at 8 °C. Crystals typically appear within 1 day and continue to grow over the course of several weeks. The largest crystals analyzed had dimensions of ≈100 × 100 × 300 μm with a hexagonal shape when viewed down their long axis. Before flash cooling, crystals grown under condition A were cryoprotected by soaking in crystallization solution A containing 9.6 mM C_8E_4 and 15% glycerol by volume. Crystals grown under condition B did not require additional cryoprotection. Crystals were flash-cooled in liquid nitrogen before X-ray exposure.

Diffraction Data Collection, Phasing, and Structural Refinement. Diffraction data were collected at the NSLS X29 and APS ID-23-D beamlines. The data were reduced by using HKL2000 (2) and TRUNCATE from the CCP4 suite (3). Because molecular replacement trials using the *Synechocystis* ACO structure (PDB ID code 2BIX) (4) failed to yield a correct solution, we attempted de novo phasing using the anomalous signal from the natively bound iron atom. A high multiplicity dataset (native 2), collected on a crystal grown under condition B at a wavelength just above the iron K edge to maximize the anomalous signal, was used to obtain initial phase estimates. $\Delta F^{\pm}$ values were calculated using SHELXC and the iron substructure was located by using data within the resolution range of 50–3 Å in SHELXD (5). Subsequent density modification in SHELXE using data to 2.5-Å resolution clearly revealed the correct heavy atom enantiomorph and the resulting electron density map had flat solvent regions and good connectivity in regions containing protein. The graphical user interface HKL2MAP was used to call SHELX programs (6). Phases were further improved by density modification in RESOLVE (7) to the point that automated model building with ARP/wARP (8) was feasible. This initial model was improved by multiple rounds of REFMAC refinement against the 2.14-Å resolution dataset collected on a crystal grown under condition A (native 1) (9, 10) and manual model adjustments using Coot (11). The stereochemical quality of the model was assessed with the Molprobity server (12). Data collection, phasing and refinement statistics are shown in Table S1 and S2. It was noted that ≈80% of screened crystals suffered from significant merohedral twinning; however, little or no twinning was detected in the datasets used for this structural analysis using XTRIAGE from the PHENIX suite (13, 14). The electron densities were well defined except in a few segments that we predict interact with membranes and may become disordered on detergent solubilization. Weak electron density was observed for residues 1–2 and 109–126, so these regions were excluded from the final model. The final model consisted of 96.3% of the total polypeptide chain. During refinement, residual $F_o - F_c$ density on two sides of the modeled Ser^{341} side chain was present, consistent with the actual presence of a Leu side chain. RPE65 alignments revealed that a Leu residue is found in this position in all other RPE65 sequences, suggesting that the Ser^{341} residue assignment in the published bovine RPE65 sequence (National

Center for Biotechnology Information accession code NP_776878) is erroneous. The bovine eyes used in this study came from a mixture of different breeds, excluding the possibility that this difference observed in our structure represents a polymorphism specific to a particular breed of cattle. Therefore, we consider Leu rather than Ser to be the wild-type residue at position 341 in the bovine RPE65 sequence.

Structural Analysis. Sequence-based alignments were produced with ClustalW (15). Structure-based alignments and 3D superpositions were produced with the DALI server (16). Contact surface area calculations were performed with the PISA server (17). MOLE was used to visualize tunnels leading to the active site iron atom (18). All structure figures were made with PyMOL v1.0 (19).

Retinoid Isomerization Activity Assay. The retinoid isomerization reaction was carried out in 10 mM Tris/HCl, pH 7.5, with addition of BSA, ATP, and apo-cellular retinaldehyde-binding protein to final concentrations of 1%, 10 mM, and 6 μM, respectively; 400 μg of RPE microsomes was used for each experimental sample. The reaction was initiated by addition of 0.6 μmol of *all-trans*-retinol in 1 μL of *N*,*N*-dimethylformamide (DMF) or *all-trans*-retinyl palmitate prebound to BSA (1). Reaction mixtures were incubated at 37 °C for 1 h in the dark before methanol/hexane extraction. The organic phase was collected and analyzed as described below.

Retinoid Extraction and Analysis. RPE microsomes or purified RPE65 solutions containing 400 μg of protein were mixed with an equal volume of methanol and extracted with 0.5 mL of hexane. The resulting organic phase was collected, dried in a SpeedVac, and redissolved in 200 μL of hexane. The retinoid composition was determined by HPLC with a Hewlett Packard 1100 series HPLC system equipped with a diode array detector and a normal phase column (5 μm, 4.5 × 250 mm; Agilent-Si) eluted with 10% ethyl acetate in hexane at a flow rate of 1.4 mL/min (20, 21).

Mass Spectrometric Analysis of RPE65. Four hundred μg of purified native bovine RPE65 was alkylated with 25 mM methylmethanethiosulfonate for 15 min at room temperature. The protein then was precipitated twice with chloroform/methanol (22). After air drying, the protein pellet was solubilized in 10 μL of formic acid and immediately diluted 10 times with water, after which 20 μL of sequencing grade pepsin (Worthington) was added at a concentration of 1 μg/μL. The sample was incubated at 30 °C overnight. Separation of RPE65 peptides was achieved with an Agilent Technologies 1100 HPLC system and a Phenomenex C-18 column (Luna, 5 μm, 20 × 2.0 mm). Samples were analyzed by a gradient of isopropanol in water (0–100% in 30 min, then 4 min at 100% isopropanol) at constant flow rate of 0.2 mL/min. All solvents contained 0.1% (vol/vol) formic acid. The effluent was directed into an ESI source of an LXQ linear ion trap mass spectrometer (Thermo Fisher Scientific). Collected mass spectra were analyzed with Xcalibur software version 2.0.7.

MS Analysis of Retinoids Produced in RPE Microsomes in the Presence of Isotopically Labeled Water. The retinoid isomerization reaction was carried out under standard conditions described above in the presence of $H_2{}^{18}O$ (50% vol/vol). The product of the reaction (11-*cis*-retinol) was purified by HPLC (10% ethyl acetate in hexane at a flow rate of 1.4 mL/min; Agilent-Si; 5 μm, 4.5 × 250 mm). Because an intact retinol molecule is difficult to analyze by LC-MS because of the loss of water on ionization, we converted the retinol products to 13,14-dihydroretinol using the enzyme retinol saturase (RetSat) before MS analysis. HEKK cells transformed with the mouse RetSat gene (23) were seeded in 24-cm^2 culture flasks, and the expression of RetSat was induced with 1 μg/mL tetracycline 48 h before analysis; 11-*cis*-retinol from the above step was dissolved in 20 μL of anhydrous *N*,*N*-DMF, exposed to bright light and added to 5 mL of growth medium consisting of DMEM, pH 7.2, with 4 mM L-glutamine, 4,500 mg/L glucose and 110 mg/L sodium pyruvate, supplemented with 10% heat-inactivated FBS, 100 units/mL penicillin, and 100 units/mL streptomycin. Cells were incubated with substrate for 6 h at 37 °C in 5% CO_2 and 100% humidity. Media and cells were collected and mixed with an equal volume of methanol. The methanol/water mixture was extracted twice with two volumes of hexane. The organic phase was combined, dried in a SpeedVac, resuspended in hexane, and analyzed by normal-phase HPLC (10% ethyl acetate in hexane at a flow rate of 1.4 mL/min; Agilent-Si; 5 μm, 4.5 × 250 mm). The peak corresponding to 13,14-dihydroretinol was collected, the solvent was evaporated, and the retinoid was redissolved in 0.25 mL of 50% acetonitrile in methanol. Then, the sample was injected onto a C-18 Eclipse XDB column; 5 μm, 4.5 × 150 mm (Agilent) equilibrated with 50% acetonitrile/methanol. The effluent was direct into an APCI source of LXQ linear ion trap (Thermo Fisher Scientific). The 13,14-dihydroretinol was eluted from the column with isocratic flow of the equilibration solvent. [^{18}O]-*all-trans*-retinol, used as a control was synthesized following the method described by McBee et al. (24).

1. Stecher H, Gelb MH, Saari JC, Palczewski K (1999) Preferential release of 11-*cis*-retinol from retinal pigment epithelial cells in the presence of cellular retinaldehyde-binding protein. *J Biol Chem* 274:8577–8585.
2. Otwinowski Z, Minor W (1997) Processing of X-ray diffraction data collected in oscillation mode. *Methods Enzymol* 276:307–326.
3. Collaborative Computational Project, Number 4 (1994) The CCp4 suite: Programs for protein crystallography. *Acta Crystallogr D* 50:760–763.
4. Kloer DP, Ruch S, Al-Babili S, Beyer P, Schulz GE (2005) The structure of a retinal-forming carotenoid oxygenase. *Science* 308:267–269.
5. Sheldrick GM (2008) A short history of SHELX. *Acta Crystallogr A* 64:112–122.
6. Pape T, Schneider TR (2004) HKL2MAP: A graphical user interface for phasing with SHELX programs. *J Appl Crystallogr* 37:843–844.
7. Terwilliger TC (2001) Maximum-likelihood density modification using pattern recognition of structural motifs. *Acta Crystallogr D* 57:1755–1762.
8. Langer G, Cohen SX, Lamzin VS, Perrakis A (2008) Automated macromolecular model building for X-ray crystallography using ARP/wARP version 7. *Nat Protoc* 3:1171–1179.
9. Murshudov GN, Vagin AA, Dodson EJ (1997) Refinement of macromolecular structures by the maximum-likelihood method. *Acta Crystallogr* 53:240–255.
10. Winn MD, Murshudov GN, Papiz MZ (2003) Macromolecular TLS refinement in REFMAC at moderate resolutions. *Methods Enzymol* 374:300–321.
11. Emsley P, Cowtan K (2004) Coot: Model-building tools for molecular graphics. *Acta Crystallogr D* 60:2126–2132.
12. Davis IW, et al. (2007) MolProbity: All-atom contacts and structure validation for proteins and nucleic acids. *Nucleic Acids Res* 35:W375–W383.
13. Zwart PH, Grosse-Kunstleve RW, Lebedev AA, Murshudov GN, Adams PD (2008) Surprises and pitfalls arising from (pseudo)symmetry. *Acta Crystallogr* 64:99–107.
14. Zwart PH, Grosse-Kunsteleve RW, Adams PD (2005) Xtraige and Fest: Automatic assessment of X-ray data and substructure structure factor estimation. *CCP4 Newsletter* 43:27–35.
15. Larkin MA, et al. (2007) Clustal W and Clustal X version 2.0. *Bioinformatics* 23:2947–2948.
16. Holm L, Kaariainen S, Rosenstrom P, Schenkel A (2008) Searching protein structure databases with DaliLite v. 3. *Bioinformatics* 24:2780–2781.
17. Krissinel E, Henrick K (2007) Inference of macromolecular assemblies from crystalline state. *J Mol Biol* 372:774–797.
18. Petrek M, Kosinova P, Koca J, Otyepka M (2007) MOLE: A Voronoi diagram-based explorer of molecular channels, pores, and tunnels. *Structure* 15:1357–1363.
19. DeLano WL (2008) The PyMOL Molecular Graphics System (DeLano Scientific, Palo Alto CA).
20. Golczak M, Kuksa V, Maeda T, Moise AR, Palczewski K (2005) Positively charged retinoids are potent and selective inhibitors of the *trans–cis* isomerization in the retinoid (visual) cycle. *Proc Natl Acad Sci USA* 102:8162–8167.
21. Golczak M, et al. (2005) Lecithin:retinol acyltransferase is responsible for amidation of retinylamine, a potent inhibitor of the retinoid cycle. *J Biol Chem* 280:42263–42273.
22. Wan J, Roth AF, Bailey AO, Davis NG (2007) Palmitoylated proteins: Purification and identification. *Nat Protoc* 2:1573–1584.
23. Moise AR, Kuksa V, Imanishi Y, Palczewski K (2004) Identification of *all-trans*-retinol:*all-trans*-13,14-dihydroretinol saturase. *J Biol Chem* 279:50230–50242.

24. McBee JK, et al. (2000) Isomerization of *all-trans*-retinol to *cis*-retinols in bovine retinal pigment epithelial cells: Dependence on the specificity of retinoid-binding proteins. *Biochemistry* 39:11370–11380.

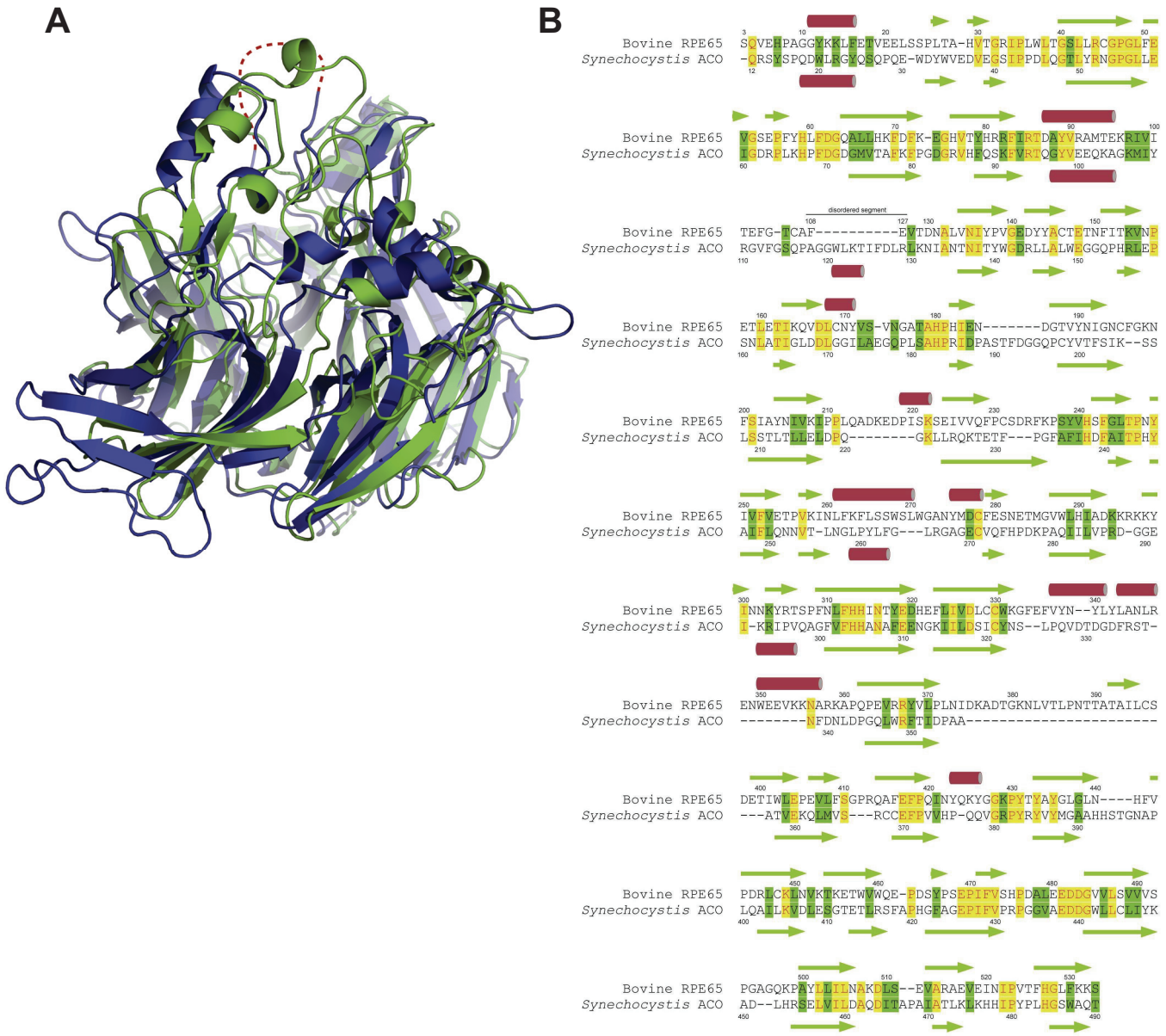

Fig. S1. Comparison of the RPE65 and ACO crystal structures. (*A*) Structural superposition of RPE65 (blue; PDB ID code 3FSN) and ACO (green; PDB ID code 2BIW). The two structures superimpose with an rmsd of 2.5 Å over 443 matched Cα positions. The most notable differences are found in the helical cap (top) of the propeller and in blade III, where RPE65 contains a ≈30 residue extension. The dashed maroon line indicates the approximate position the disordered loop in RPE65 consisting of residues 109–126. (*B*) A structure-based alignment of bovine RPE65 and *Synechocystis* ACO amino acid sequences. Red cylinders and green arrows represent helices and strands, respectively. Yellow and green letter highlighting indicate sequence identity and conservation, respectively. The alignment was performed with the DALI server.

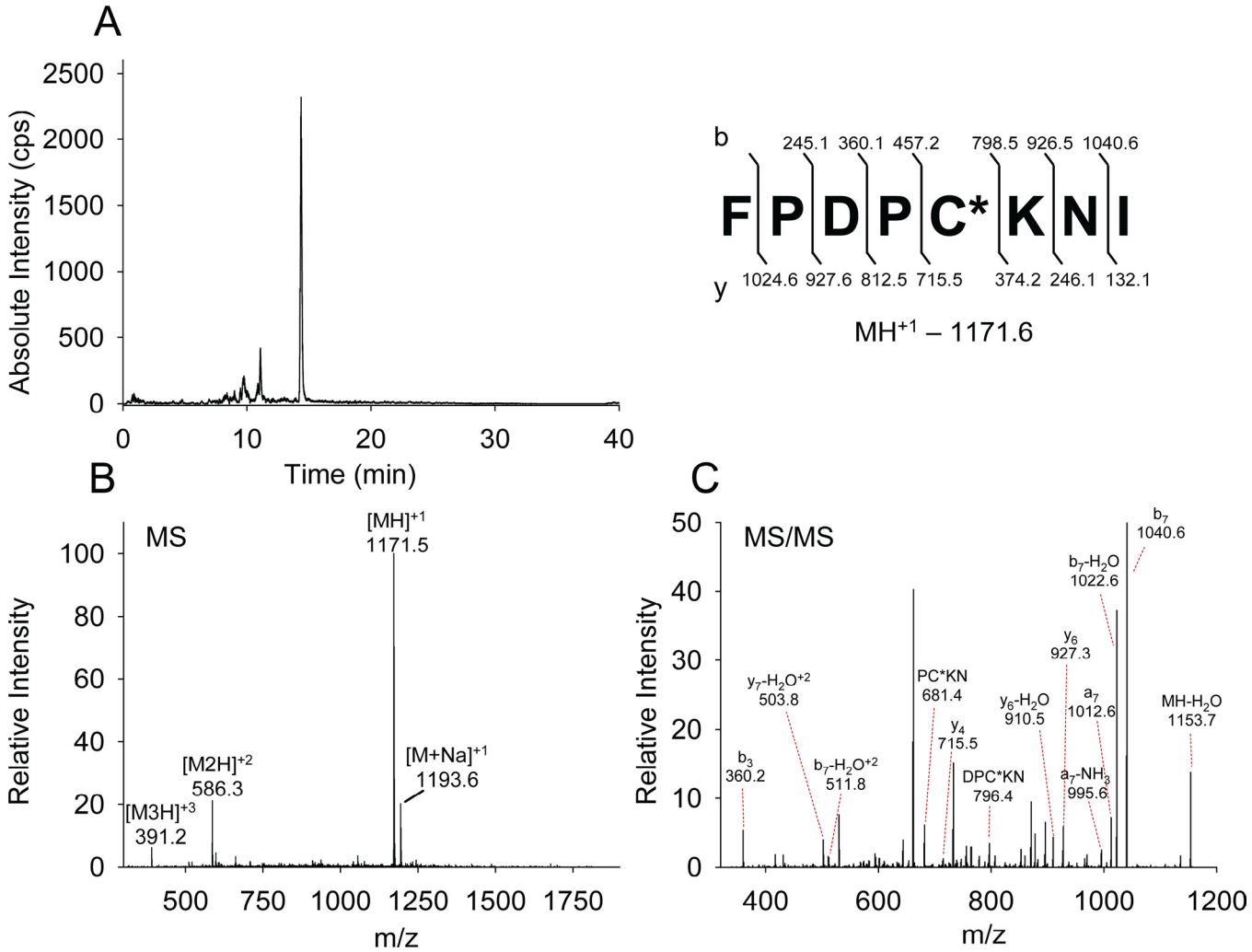

Fig. S2. Identification of palmitoylation on Cys[112] in native bovine RPE65. Four hundred micrograms of RPE65 was digested with pepsin and the resulting peptides were analyzed by LC-MS. (*A*) Elution profile (a) of palmitoylated peptide (residues 108–115) represented as extracted ion chromatogram at $m/z = 1171.7$ corresponding to a singly charged peptide. (*B*) MS spectra of peptides eluted at 14 min. Singly, doubly, and triply charged peptides were identified. (*C*) Fragmentation pattern (MS^2) of a single charged ion. Identified ions and amino acids characteristic of palmitoylated peptides are labeled.

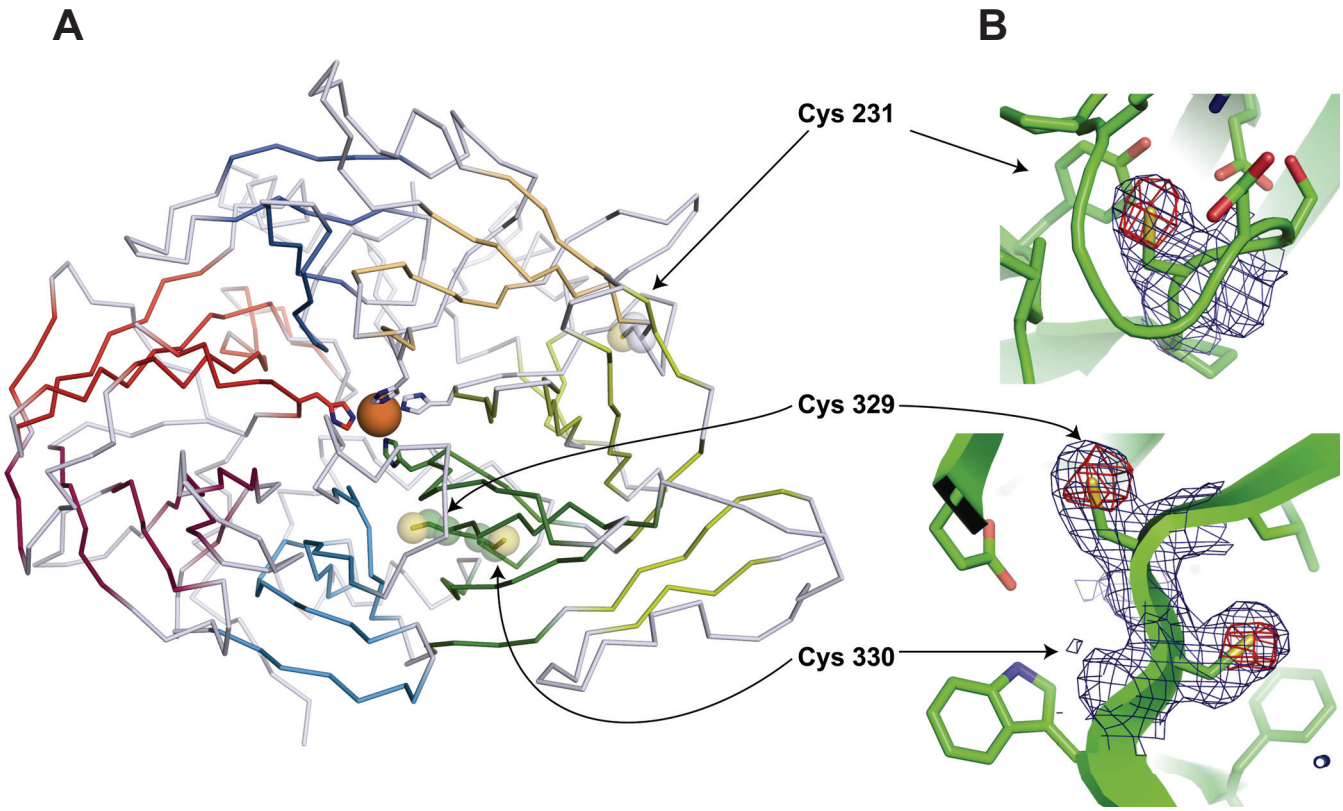

Fig. S3. Locations of and electron density maps surrounding the cysteine residues previously proposed to participate in a palmitoylation switch mechanism. (*A*) Locations of Cys residues 231, 329, and 330 in the RPE65 structure. None of the sulfur atoms of these residues are surface exposed or located on the predicted membrane binding face of the protein. (*B*) Crystallographic determination of the palmitoylation status of Cys residues 231, 329, and 330. The blue mesh represents the final σ A-weighted $2F_o - F_c$ electron density map contoured at 1 σ. There are no signs of residual density that could represent a palmitoyl group. The red mesh represents a 4-σ NCS-averaged anomalous difference electron density map calculated using the anomalous differences from the native 2 dataset and the refined phases. The latter map confirms the correct positioning of the Cys sulfur atoms.

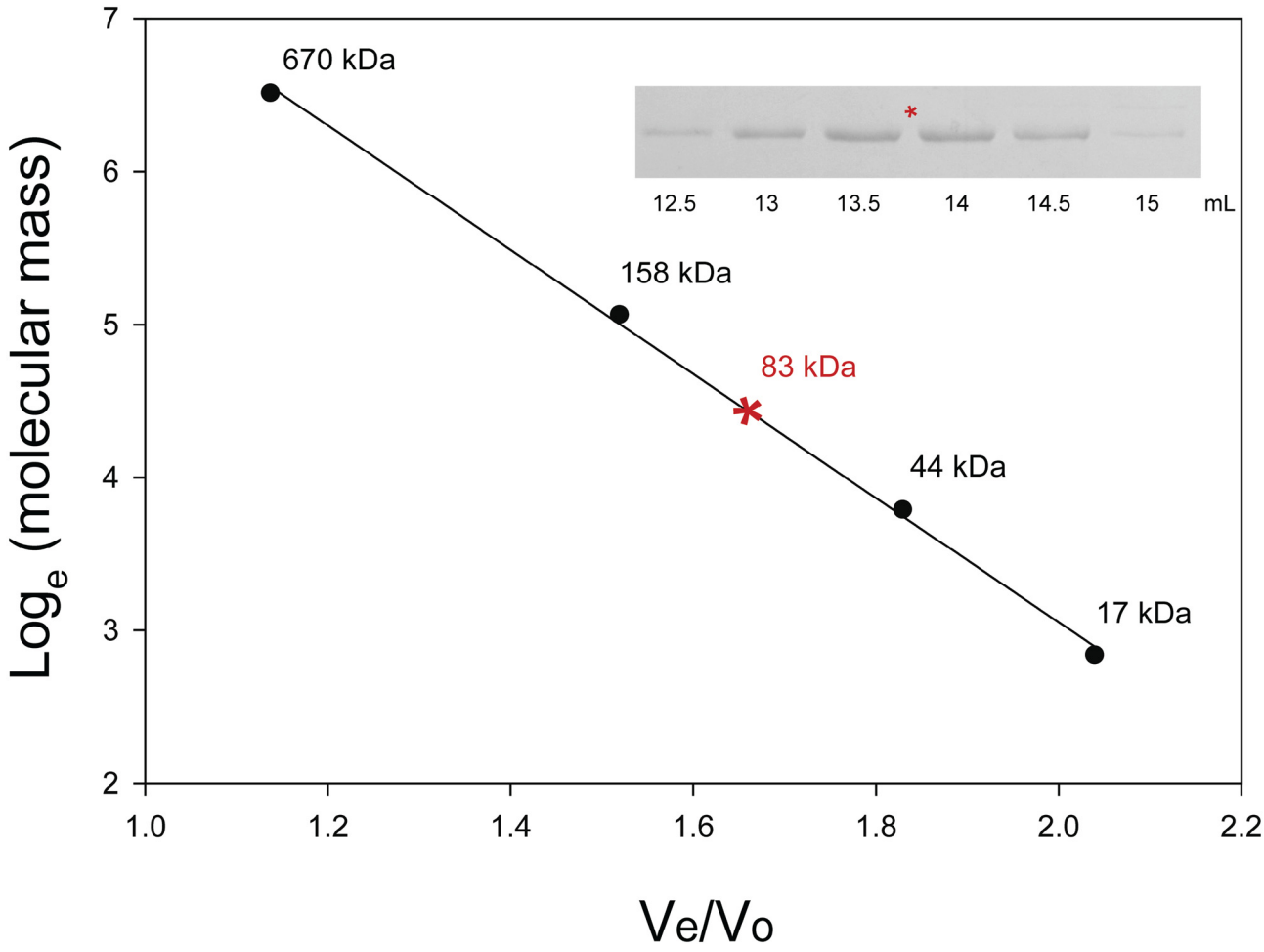

Fig. S4. Gel filtration analysis of purified RPE65. The black dots represent the elution values obtained for the standards on a Superdex 200 10/300 gel filtration column. RPE65 eluted at an apparent molecular mass of 83 kDa (red asterisk) as shown by SDS/PAGE analysis (*Inset*) of the gel filtration eluates, which is consistent with an RPE65 monomer complexed with a detergent micelle. V_e/V_o, elution volume/void volume.

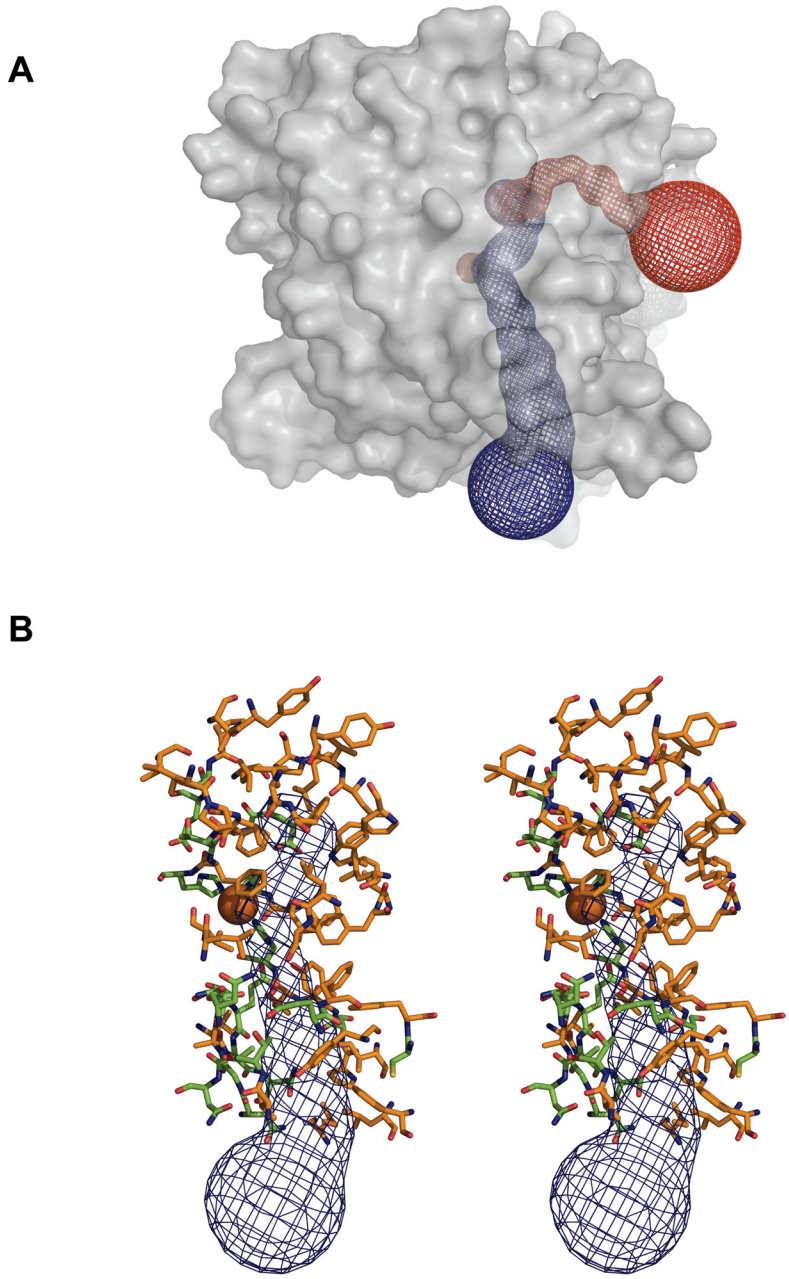

Fig. S5. The two tunnels that lead to the active site iron of RPE65. (*A*) The blue mesh represents the hydrophobic, substrate entry/product exit tunnel (tunnel A) and the red mesh represents the narrow hydrophilic tunnel (tunnel B). (*B*) Stereoview of the residues that line tunnel A. The carbon atoms of hydrophobic residues and polar or charged residues are colored orange and green, respectively. The iron atom is shown as a brown sphere in both panels.

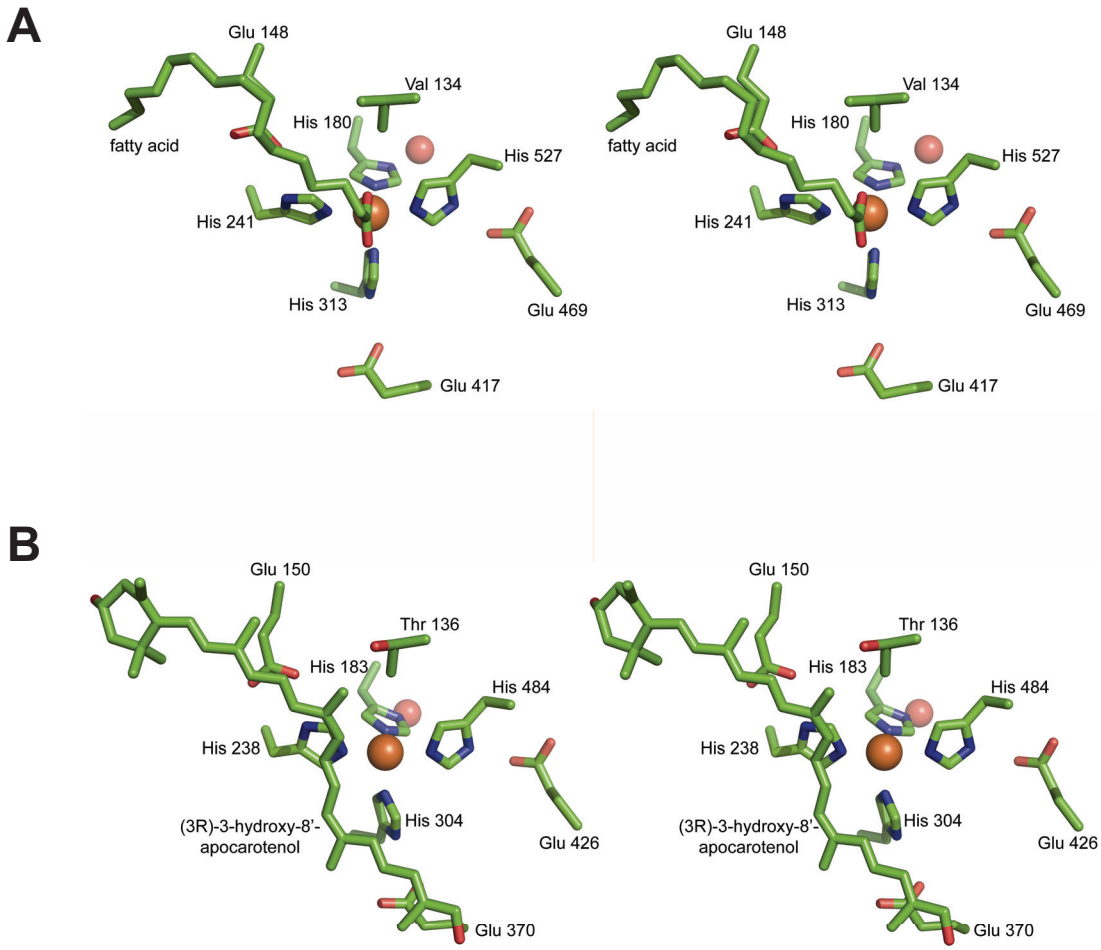

Fig. S6. Stereoview of the iron cofactor and its ligands and the putative substrates/products in the active sites of RPE65 (*A*) and ACO (*B*). The conformations of the first and second shell iron ligands are quite similar between structures. The non-protein ligands occupy similar positions with respect to the iron centers except that the apocarotenol substrate does not directly interact with the iron ion in the ACO structure.

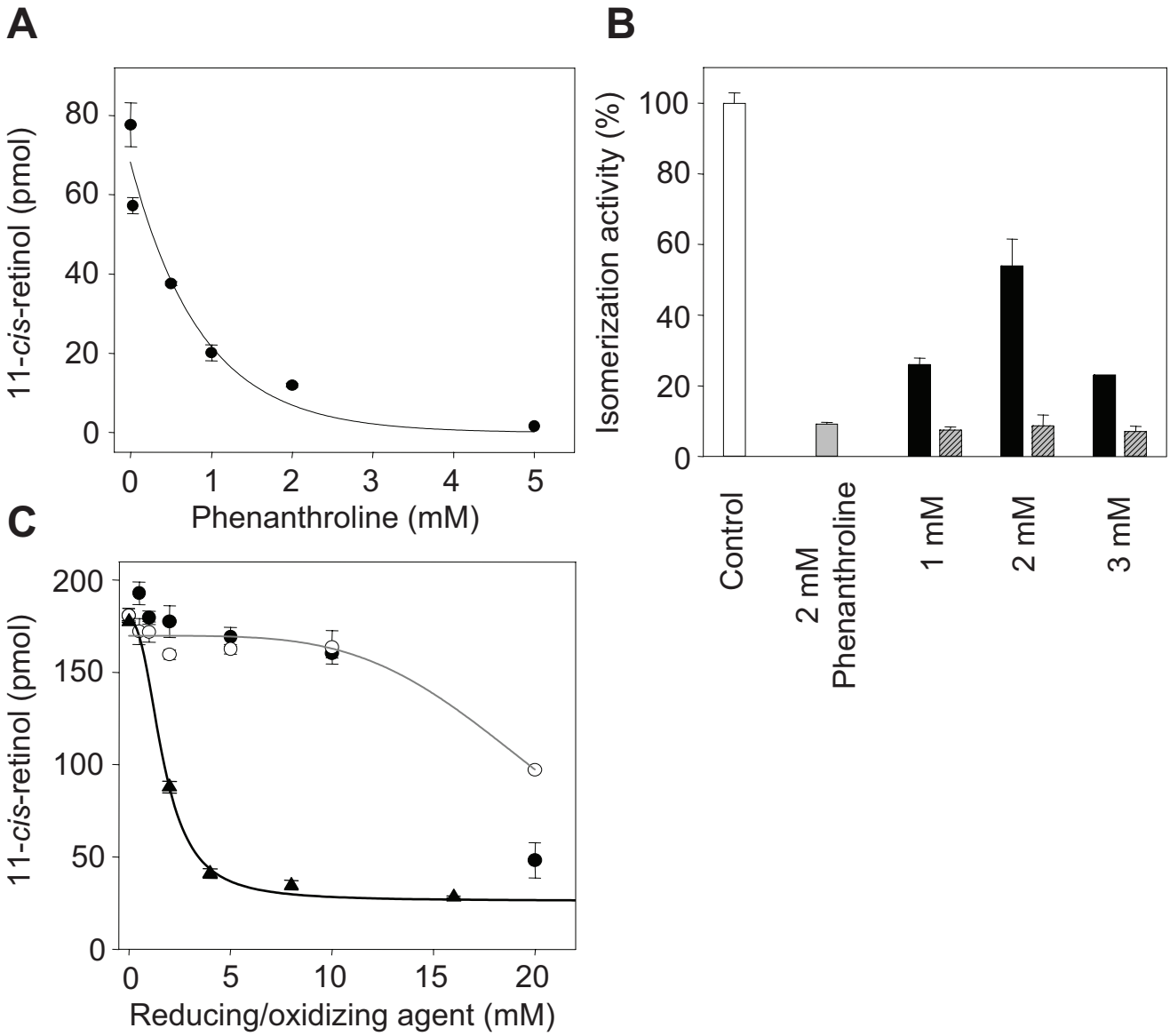

Fig. S7. Effect of ion chelator, reducing/oxidizing reagents and metal ion on retinoid isomerase activity. (*A*) The 1,10-phenanthroline concentration-dependent inhibition of 11-*cis*-retinol generation. Bovine RPE microsomal proteins (100 μg) were preincubated for 15 min at room temperature with increasing concentrations of the ion chelator before addition of cellular retinaldehyde binding protein (CRALBP) and *all-trans*-retinol; 11-*cis*-retinol generation was analyzed by HPLC. Amounts of 11-*cis*-retinol were calculated from peak areas. (*B*) Effect of iron ions on isomerase activity. Bovine RPE microsomes were preincubated with 2 mM of 1,10-phenanthroline. To restore isomerase activity, reactions were performed in the presence of varying concentrations of $FeSO_4$ (black bars) or $FeCl_3$ (gray striped bars). (*C*) Dependence of retinoid isomerization activity on the concentrations of reducing reagents, sodium dithionite (open circles) and ascorbic acid (filled circles) or the oxidizing agent, hydrogen peroxide (triangles). Bovine RPE microsomes were incubated with increasing concentrations of these reagents for 5 min before initiation of enzymatic reaction by addition of *all-trans*-retinol and CRALBP.

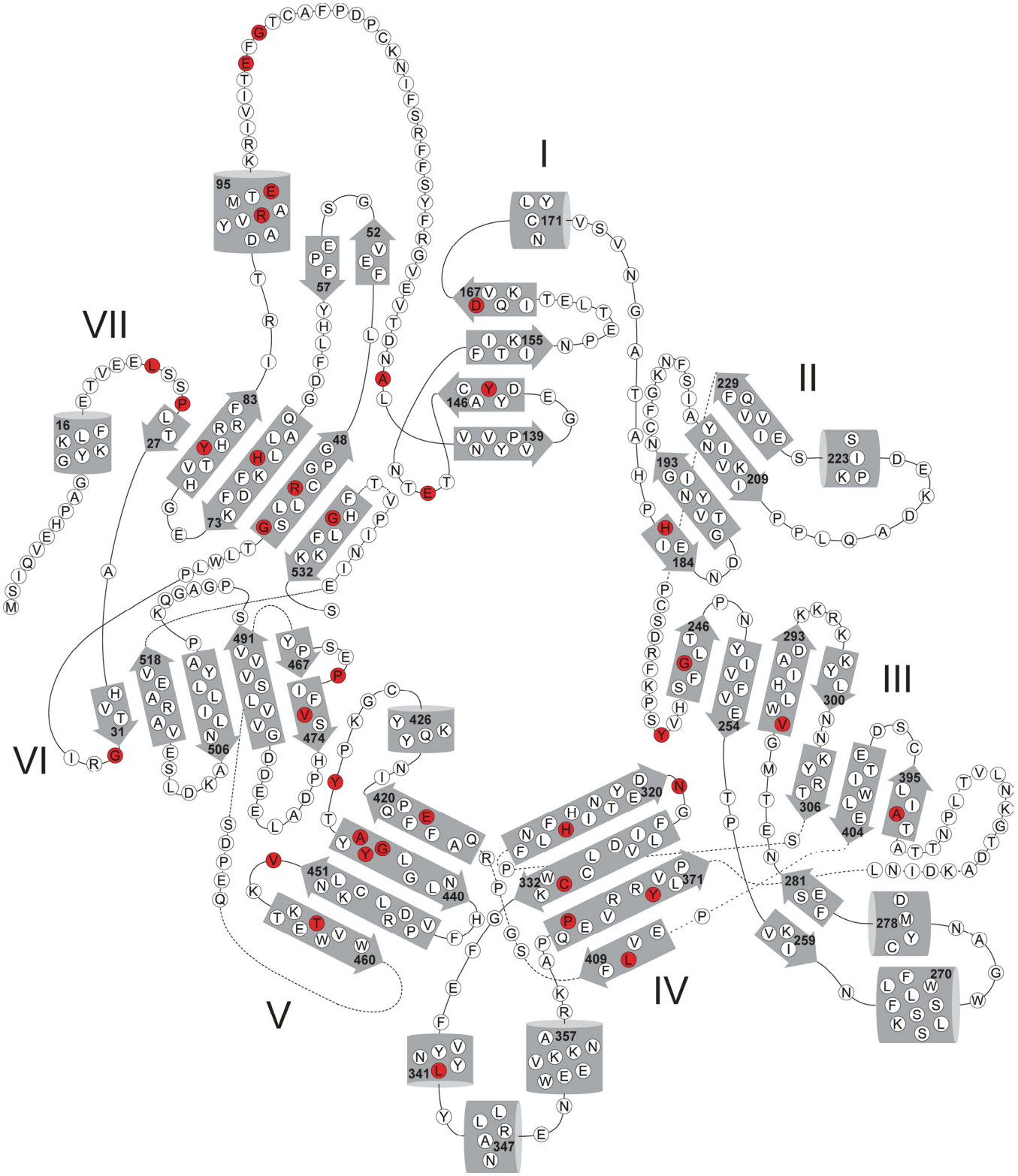

Fig. S8. LCA or RP-associated RPE65 amino acid substitutions. An RPE65 topology diagram showing amino acid positions found to be substituted in LCA or RP patients (colored in red). The human RPE65 sequence is shown. The numbers indicate the position in the RPE65 amino acid sequence of the C-terminal residue in each secondary structure element.

Table S1. Data collection

Crystal	Native 1	Native 2 (Fe-SAD)*
Beamline	APS 23-ID-D	NSLS X29
Wavelength, Å	1.03324	1.74100
Space group	$P6_5$	$P6_5$
Resolution, Å	50–2.14 (2.22–2.14)	50–2.5 (2.59–2.50)
Unit cell parameters a = b, c, Å	176.53, 86.87	176.94, 86.96
Mosaicity, °	0.42	0.38
Unique reflections	83,509	53,648
Completeness, %	99.5 (98.3)	99.6 (99)
Multiplicity	6.3 (5.7)	18.2 (9.3)
$I/\sigma(I)$	14.2 (2.16)	31 (3.29)
R_{sym} on I, %†	11.6 (73.4)	11.5 (65.6)
Wilson B, Å^2	32	54
Monomers per asymmetric unit	2	2
Solvent content, %	62	62
SAD phasing		
Sites per asymmetric unit	NA	2
FOM before/after statistical density modification	NA	0.127/0.725

Values in parentheses are for the highest-resolution shell of data. APS, Advanced Photon Source; FOM, figure of merit; ID, insertion device; NSLS, National Synchrotron Light Source; SAD, single-wavelength anomalous dispersion; NA, not applicable.

*Bijvoet pairs unmerged.

†$R_{sym}(I) = \Sigma_{hkl}\Sigma_i |I_i(hkl) - \langle I(hkl)\rangle|/\Sigma_{hkl}\Sigma_i I_i(hkl)$ with summation performed over all symmetry-equivalent reflections excluding those observed only once.

Table S2. Refinement

Dataset	Native 1
Resolution range, Å	48.22–2.14
Unique reflections	80,559
Total refined atoms	8,636
Protein	8,334
Water	274
Iron	2
PEG 200	26
B factors, Å^2	
Protein*	35.9
Water	34.7
Iron	27.1
PEG 200	59.35
Rmsd bond lengths, Å	0.013
Rmsd bond angles, °	1.4
R_{work}, %	18
R_{free}, %	21.6
Ramachandran plot (Molprobity)	
Favored, %	97.2
Outliers, %	0

$R_{work} = \Sigma \, | \, |F_{obs}| - |F_{calc}| \, | \, / \, \Sigma \, |F_{obs}|$. R_{free} was calculated exactly as R_{work} using 4,299 (5.1%) randomly selected reflections that were omitted from refinement.

*Residual *B* factors after translation, libration, screw (TLS) refinement.